SIViP (2012) 6:503–511
DOI 10.1007/s11760-012-0334-0

ORIGINAL PAPER

1-D and 2-D digital fractional-order Savitzky–Golay differentiator

Dali Chen · YangQuan Chen · Dingyu Xue

Received: 10 September 2011 / Revised: 6 March 2012 / Accepted: 11 March 2012 / Published online: 17 May 2012

Abstract In this paper, the one-dimension digital fractional-order Savitzky–Golay differentiator (DFOSGD), which generalizes the Savitzky–Golay filter from the integer order to the fractional order, is introduced and extended to 2-D by a group of direction operators. Then, a new image-enhancing algorithm is proposed based on the 2-D DFOSGD, and an unsupervised optimization algorithm is proposed for choosing the fractional-order parameter. Four numerical experiments are used to assess the performance of 2-D DFOSGD-based image-enhancing algorithm, and the results demonstrate its validity.

Keywords Fractional-order derivative · Digital differentiator · Savitzky–Golay filter · Image enhancement

1 Introduction

Fractional differentiation, a mathematical discipline dealing with the differentiation of arbitrary order, was proposed in the seventeenth century and developed mainly in the nineteenth century [1]. Many definitions of fractional differentiation have been proposed, and the most popular definitions among them involve Riemann–Liouville definition [2], Grünwald–Letnikov definition [3], and Caputo definition [4]. The digital fractional-order differentiator (DFOD) is a very useful tool to estimate the fractional derivatives of a given signal. In 2001, an excellent survey, which summarized and compared some fractional-order operators for implementing fractional-order controllers, was presented in [5]. In 2002, some DFODs were discussed for the continuous models in [6]. These methods included Carlson's method [7], Dutta Roy's method [8], Chareff's method [9], Matsuda's method [10], and Oustaloup's method [11]. For discrete time case, some FIR filters were presented in [12,13]. However, the FIR approximation may lead to very high order of FIR filters. Hence, some infinite impulse response (IIR) filters were proposed [14–19]. These methods include fractional differencing formula, Taylor series expansion method, Tustin method, continued fraction expansion, least-squares method, and generalized mean method. However, the existing digital fractional-order differentiators are sensitive to the noisy signal [20]. When the given signal is contaminated by the noise, the performance of the DFOD will be unsatisfactory. In order to resolve this problem, a digital fractional-order Savitzky–Golay differentiator (DFOSGD), which generalizes the Savitzky–Golay digital differentiator from the integer order to the fractional order using Riemann–Liouville fractional-order derivative definition, was proposed [21]. And the detailed implementation method is introduced in this paper.

Recently, more and more fractional differentiation–based methods were applied in the fields of image processing [22–26]. In this paper, we aim our interests at the image enhancement. The integer-order differential mask is an important tool in edge enhancement, but it also damages the texture detail feature of image. The texture detail feature of image often has fractal-like structure, and fractional differentiation is an effective tool to deal with this fractal problem. Based on

D. Chen · D. Xue
College of Information Science and Engineering,
Northeastern University, Shenyang 110006, Liaoning, China
e-mail: chendali@ise.neu.edu.cn

D. Xue
e-mail: xuedingyu@mail.neu.edu.cn

Y. Chen (✉)
Department of Electrical and Computer Engineering,
Center for Self-Organizing and Intelligent Systems (CSOIS),
Utah State University, Logan, UT, 84322-4160, USA
e-mail: yqchen@ece.usu.edu

this fact, six fractional differentiation–based image enhancement masks were proposed by [27]. But how to optimize the fractional order is still unsolved. In order to solve this problem, we generalized the DFOSGD from one dimension to two dimension and proposed an adaptive image-enhancing method based on 2-D DFOSGD mask. Moreover, an unsupervised algorithm also was proposed to optimize the fractional-order parameter. The simulating results demonstrated that the 2-D DFOSGD can be used to enhance the image effectively.

The outline of this paper is as follows. In Sect. 2, the detailed implementation of 1-D DFOSGD is introduced. In Sect. 3, a group of directional templates are defined to generalize DFOSGD from one dimension to two dimension, and then the image-enhancing strategy based on the proposed 2-D DFOSGD mask is described in detail. Moreover, an unsupervised algorithm is also introduced. Numerical experiments are presented in Sect. 4, and the paper is concluded in Sect. 5.

2 1-D digital fractional-order Savitzky–Golay differentiator

In order to describe the general problem more clearly, we define the problem in full details here. Given uniformly sampled signal $y(j)$, we wish to smooth and estimate its dnth-order derivative with an I-point filtering window and an n-degree polynomial. For the original Savitzky–Golay filter, dn is a non-negative integer and $n < I$, so that the least-squares polynomial can be obtained by

$$f_n(i) = \sum_{k=0}^{n} b_k i^k, \tag{1}$$

where $f_n(i)$ is a n-degree polynomial function that is used to fit the given signal, $i = 1, 2, \ldots, I$ is the position of the ith point in the filtering window, and b_k is the kth coefficient of the polynomial function. In order to estimate the coefficient b_k accurately, the least-squares method is used. For better readability, we will use matrix notation to describe this problem, and Eq. (1) can be rewritten by

$$Y = XB + \varepsilon, \tag{2}$$

where $Y = [y_1, y_2, \ldots, y_I]^T$ denotes the measured signal points in the filtering window, $B = [b_0, b_1, \ldots, b_n]^T$ denotes the coefficient vector of the polynomial function, ε is the estimation error, and X is an $I \times (n+1)$ Vandermonde matrix defined by

$$X = \begin{bmatrix} 1 & 1^1 & \ldots & 1^n \\ 1 & 2^1 & \ldots & 2^n \\ \vdots & \vdots & \vdots & \vdots \\ 1 & I^1 & \ldots & I^n \end{bmatrix}. \tag{3}$$

The coefficients of the best-fit polynomial can be obtained by minimizing the sum of the squared errors between the actual data and the fitting points. Hence, we can obtain

$$B = (X^T X)^{-1} X^T Y. \tag{4}$$

Using the resulting B, we can get the estimation of the given signal by

$$\widehat{Y} = XB = X(X^T X)^{-1} X^T Y = WY, \tag{5}$$

where W denotes the moving window's coefficient matrix that can be used to smooth the given signal. Using the coefficient matrix W, we can compute all the smoothing values in the filtering window. If we want to estimate the ith point in the filtering window, we can use the ith element of W.

The integer-order derivatives of the polynomial function $f_n(i)$ are given by

$$\begin{aligned} df_n(i)/di &= b_1 + 2b_2 i + \cdots + nb_n i^{n-1} \\ d^2 f_n(i)/di^2 &= 2b_2 + \cdots + n(n-1)b_n i^{n-2}. \\ &\cdots \\ d^n f_n(i)/di^n &= n! b_n \end{aligned} \tag{6}$$

Hence, the dnth-order derivative of the ith point in the given signal can be estimated by

$$\begin{aligned} \widehat{Y_i^{(dn)}} &= X_i^{(dn)} B = W_i^{(dn)} Y \\ &= \left[\underbrace{0, \ldots, 0}_{dn}, dn!, \ldots, P_n^{dn} i^{n-dn} \right] (X^T X)^{-1} X^T Y, \end{aligned} \tag{7}$$

here $Y_i^{(dn)}$ denotes the dnth derivative of the ith point in the filtering window, $W_i^{(dn)}$ denotes the dnth derivative coefficient vector of the ith point in the filtering window and the permutation $P_n^{dn} = n!/(n-dn)!$. When dn is 0, Eq. (7) is equivalent to Eq. (5) and can smooth the given signal. Actually, the purpose of the original Savitzky–Golay filter is to estimate the $W_i^{(dn)}$, which can be used to calculate the dnth-order derivative of any given signal.

In this paper, the Riemann–Liouville fractional-order derivative definition in the following is used to generalize the Savitzky–Golay differentiator from the integer order to the fractional order,

$${}_a D_x^{\alpha} f(x) = \frac{1}{\Gamma(n-\alpha)} \frac{d^n}{dx^n} \int_a^x (x-t)^{n-\alpha-1} f(t) \mathrm{d}t, \tag{8}$$

where $0 \le n-1 < \alpha < n$ and $\Gamma(n-\alpha)$ is the Gamma function. Assuming the signal $f(x) = x^k$, $k \ge 0$, $x \ge 0$, then we can obtain

$${}_0 D_x^{\alpha} x^k = \frac{\Gamma(k+1)}{\Gamma(k+1-\alpha)} x^{k-\alpha}. \tag{9}$$

Here, we will introduce some useful properties. Firstly, when α is positive and integer, the fractional-order operation

is equivalent to the integer-order differentiator defined by

$$ {}_aD_x^{\alpha} f(x) = \frac{d^{\alpha} f(x)}{dx^{\alpha}}, \quad \alpha \text{ is integer.} \tag{10} $$

Secondly, the operation is linear and can be computed by

$$ {}_aD_x^{\alpha}(Mf(x) + Ng(x)) = M\ {}_aD_x^{\alpha} f(x) + N\ {}_aD_x^{\alpha} g(x). \tag{11} $$

Because of these properties, we can compute the fractional-order derivative of Eq. (1) using Eq. (9). In this way, we can generalize the SG filter from the integer order to the fractional order using Eqs. (7) and (9). The final result can be obtained by

$$ \begin{aligned} \widehat{Y_i^{(\alpha)}} &= X_i^{(\alpha)} B = W_i^{(\alpha)} Y \\ &= \left[\frac{1}{\Gamma(1-\alpha)} i^{-\alpha}, \frac{1}{\Gamma(2-\alpha)} i^{1-\alpha}, \frac{\Gamma(3)}{\Gamma(3-\alpha)} i^{2-\alpha}, \right. \\ &\quad \left. \ldots, \frac{\Gamma(n+1)}{\Gamma(n+1-\alpha)} i^{n-\alpha} \right] (X^T X)^{-1} X^T Y, \end{aligned} \tag{12} $$

and it is the generalization of Eq. (7). When α is a non-negative integer, Eq. (12) is equal to Eq. (7).

3 2-D DFOSGD-based image-enhancing algorithm

3.1 Generalization

In this section, the method generalizing the digital fractional-order Savitzky–Golay differentiator from 1-D to 2-D is introduced. In order to describe the process more clearly, some basic definitions need to be given firstly. Assume the filtering window's size $I = 2m + 1$, and m is a positive integer. Based on Eq. (12), the αth-order derivative of the middle point in the filtering window can be estimated by

$$ W_{m+1}^{(\alpha)} = [W(1), W(2), \ldots, W(2m+1)]. \tag{13} $$

However, we find two problems when we apply the $W_{m+1}^{(\alpha)}$ in 2-D image processing. The first problem is that the sum of $W_{m+1}^{(\alpha)}$ is not equal to 1 for non-integer α. This characteristic of DFOSGD changes the distribution of image pixel value and results in some bad effects. Here, the typical normalization method is used to resolve this problem. The second problem is that $W_{m+1}^{(\alpha)}$ is anisotropic and only can be used to calculate the fractional-order derivative in one direction. So, it is not effective to estimate the fractional-order derivative of image. An idea, inspired by the Kirsch's templates [28], is to define a group of templates in eight different directions and then use these templates to calculate the fractional-order derivative of image. Figure 1 shows the 2-D DFOSGD templates in the different directions including $W_{x+}^{(\alpha)}$, $W_{x-}^{(\alpha)}$, $W_{y+}^{(\alpha)}$, $W_{y-}^{(\alpha)}$, $W_{\searrow}^{(\alpha)}$, $W_{\nwarrow}^{(\alpha)}$, $W_{\nearrow}^{(\alpha)}$, and $W_{\swarrow}^{(\alpha)}$.

Let $G(x, y)$ denote the gray value of the position (x, y) in the image G. Using the 2-D DFOSGD templates, the αth-order derivatives of $G(x, y)$ in the different directions can be calculated by

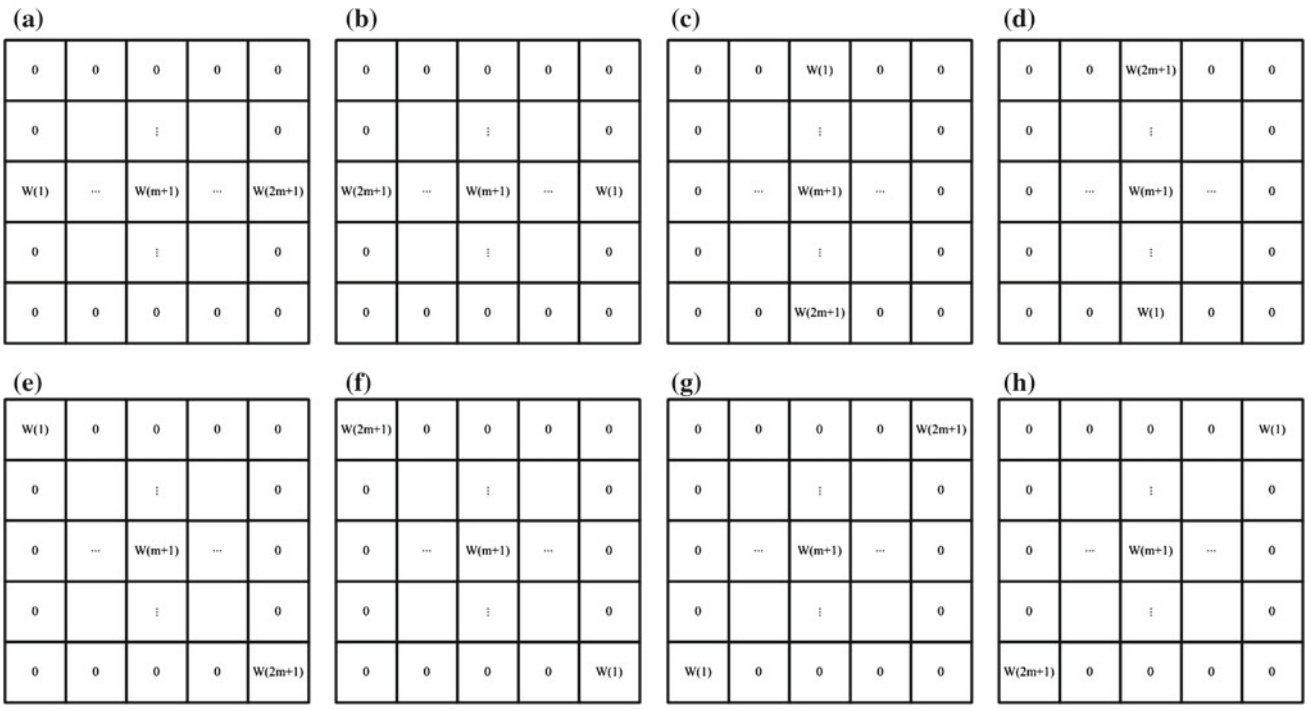

Fig. 1 2-D DFOSGD templates. **a** $W_{x+}^{(\alpha)}$, **b** $W_{x-}^{(\alpha)}$, **c** $W_{y+}^{(\alpha)}$, **d** $W_{y-}^{(\alpha)}$, **e** $W_{\searrow}^{(\alpha)}$, **f** $W_{\nwarrow}^{(\alpha)}$, **g** $W_{\nearrow}^{(\alpha)}$, **h** $W_{\swarrow}^{(\alpha)}$

$$G^{(\alpha)}_{x^+}(x,y)=\sum_{k=-m}^{m}\sum_{l=-m}^{m}W^{(\alpha)}_{x+}(k,l)G(x-k,y-l),$$

$$G^{(\alpha)}_{x^-}(x,y)=\sum_{k=-m}^{m}\sum_{l=-m}^{m}W^{(\alpha)}_{x-}(k,l)G(x-k,y-l),$$

$$G^{(\alpha)}_{y^+}(x,y)=\sum_{k=-m}^{m}\sum_{l=-m}^{m}W^{(\alpha)}_{y+}(k,l)G(x-k,y-l),$$

$$G^{(\alpha)}_{y^-}(x,y)=\sum_{k=-m}^{m}\sum_{l=-m}^{m}W^{(\alpha)}_{y-}(k,l)G(x-k,y-l),$$

$$G^{(\alpha)}_{\searrow}(x,y)=\sum_{k=-m}^{m}\sum_{l=-m}^{m}W^{(\alpha)}_{\searrow}(k,l)G(x-k,y-l),$$

$$G^{(\alpha)}_{\nwarrow}(x,y)=\sum_{k=-m}^{m}\sum_{l=-m}^{m}W^{(\alpha)}_{\nwarrow}(k,l)G(x-k,y-l),$$

$$G^{(\alpha)}_{\nearrow}(x,y)=\sum_{k=-m}^{m}\sum_{l=-m}^{m}W^{(\alpha)}_{\nearrow}(k,l)G(x-k,y-l),$$

$$G^{(\alpha)}_{\swarrow}(x,y)=\sum_{k=-m}^{m}\sum_{l=-m}^{m}W^{(\alpha)}_{\swarrow}(k,l)G(x-k,y-l).$$

Based on the fractional-order derivatives in the eight directions, the αth-order derivatives of $G(x,y)$ can be defined by

$$G^{(\alpha)}(x,y)=Sat(\max\{G^{(\alpha)}_{d}(x,y)|d\in\Omega\}), \tag{14}$$

where

$\Omega:=\{x^+,y^+,x^-,y^-,\searrow,\nwarrow,\nearrow,\swarrow\}$, and $Sat(u)$ is the saturated function defined by

$$Sat(u)=\begin{cases}0, & u<0\\ u, & u\in[0,L],\\ L, & u>L\end{cases} \tag{15}$$

here, L is the gray level of image G. For instance, $L=255$ when G is an 8-bit gray image.

Moreover, the 2-D DFOSGD-based image-enhancing algorithm is also applicable in the color image. We all know that the RGB color model is the most popular color model. However, the 'R', 'G', and 'B' components have strong coupling. If we use Eq. (14) in 'R', 'G', and 'B' channels directly, it will result in the color distortion. Lab color model is the one of the typical color models. In Lab color model, the 'L', 'a', and 'b' components have weak coupling. So, we use Lab color model instead of RGB color model to prevent the color distorted. The main process is as follows. Firstly, we transform RGB color model into Lab color model. Then, we only process the 'L' component using Eq. (14) because the 'L' component closely matches human perception of lightness. Finally, we transform the processed Lab color model back to RGB color model.

3.2 Unsupervised optimization algorithm for the fractional-order parameter

The histogram is an important tool to analyze the statistical character of digital image. Figure 2 shows the histograms

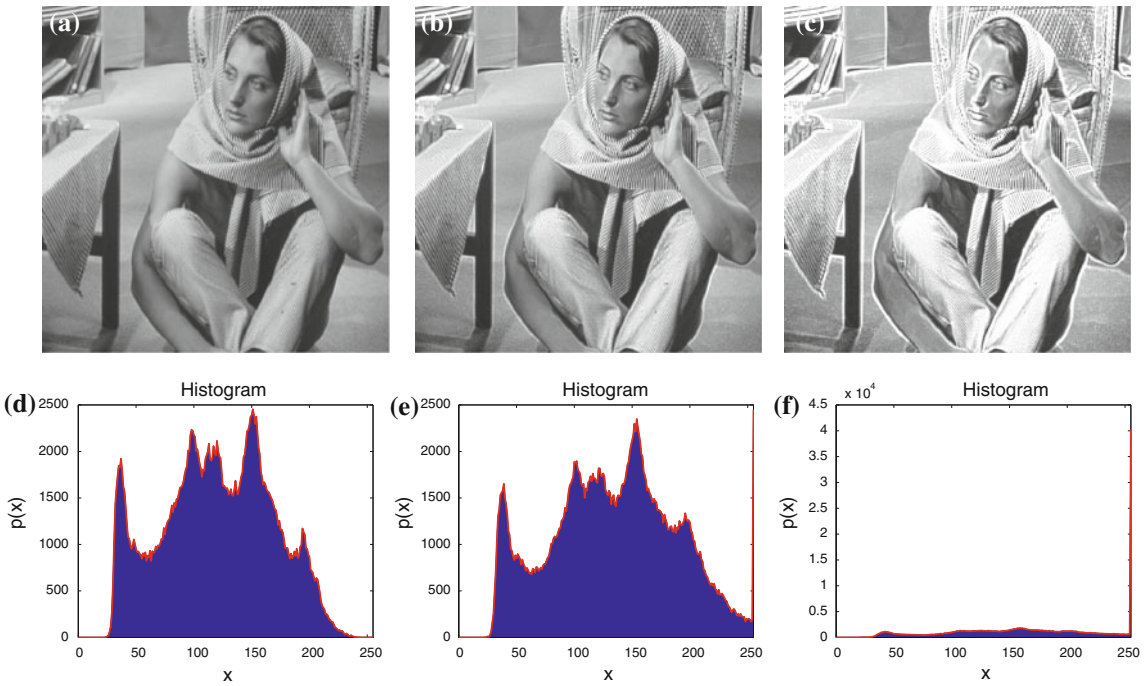

Fig. 2 Enhanced images and histograms. **a** Enhanced image with $\alpha=0.1$. **b** Enhanced image with $\alpha=0.4$. **c** Enhanced image with $\alpha=0.8$. **d** Histogram with $\alpha=0.1$. **e** Histogram with $\alpha=0.4$. **f** Histogram with $\alpha=0.8$

of the enhanced images with the different fractional orders. avg is the average intensity of the original image G and $\Omega^{(\alpha)} := \{(x, y)|G^{(\alpha)}(x, y) = L\}$ is the saturated pixel set of the enhanced image $G^{(\alpha)}$. $N^{(\alpha)}$ is the number of the element in $\Omega^{(\alpha)}$. From Fig. 2, it can be seen that $N^{(\alpha)}$ increases when α increases. When $N^{(\alpha)}$ is small, the image is owe enhanced. On the contrary, the image is over-enhanced when $N^{(\alpha)}$ is large. $N^{(\alpha)}$ can reflect the degree of enhancement very well. Based on this fact, an unsupervised method for optimizing the fractional-order parameter α is proposed. The cost function is defined as follows:

$$J(\alpha) = \sum_{(x,y)\in\Omega^{(\alpha)}} |G^{(\alpha)}(x, y) - G(x, y) - M(avg)|/N^{(\alpha)}, \tag{16}$$

where $M(x)$ is defined by

$$M(x) = \begin{cases} (\frac{x}{5})^2, & x \in [0, 25] \\ 50 - (\frac{x-50}{5})^2, & x \in [25, 150] \\ 50, & x \in [50, 150], \\ \frac{250-x}{2}, & x \in [150, 250] \\ 0, & x \in [250, 255] \end{cases} \tag{17}$$

and optimal fractional-order parameter α^* is estimated by

$$J(\alpha^*) = \min_{\alpha} J(\alpha). \tag{18}$$

In the next section, some experiments are presented to validate the proposed adaptive 2-D DFOSGD-based image-enhancing algorithm.

4 Numerical experiments

4.1 Experiment 1

In this experiment, four different kinds of images are given to evaluate the proposed 2-D DFOSGD-based image-enhancing algorithm. The optimal fractional-order α is estimated by Eq. (18). Figure 3 shows the comparison results between original image and enhanced image. Figure 3a shows a part of "Lake Tahoe" image, which is a remote sensing image captured above the Lake Tahoe and downloadable from [29]. It is obvious that some important detail information, such as street, building, and vegetation, have very bad observability. Figure 3b shows the enhanced image that is calculated by the proposed 2-D DFOSGD-based image-enhancing method with $\alpha = 0.29$, and α is estimated by Eq. (18). In the figure, the contrast is much better than the original image, and the road, building, and vegetation can be distinguished easily. Figure 3c is a cutdown photograph of snow-covered volcanoes on Russia Kamchatka Peninsula, which includes the abundant natural scene features such as lake, sea, river, stratovolcanoes, mountain, and snow, downloadable from [29]. However, the photograph is smoothed a lot because of the cutdown operation. The enhanced result, calculated by the 2-D DFOSGD-based image-enhancing method with $\alpha = 0.47$, is shown in Fig. 3d. And α also is estimated by Eq. (18). From the figure, we can see that the contrast of some detail information is enhanced greatly, especially mountain ridge, gully, and river. Figure 3e shows a part of the moon photograph downloaded from [30], and Fig. 3f shows

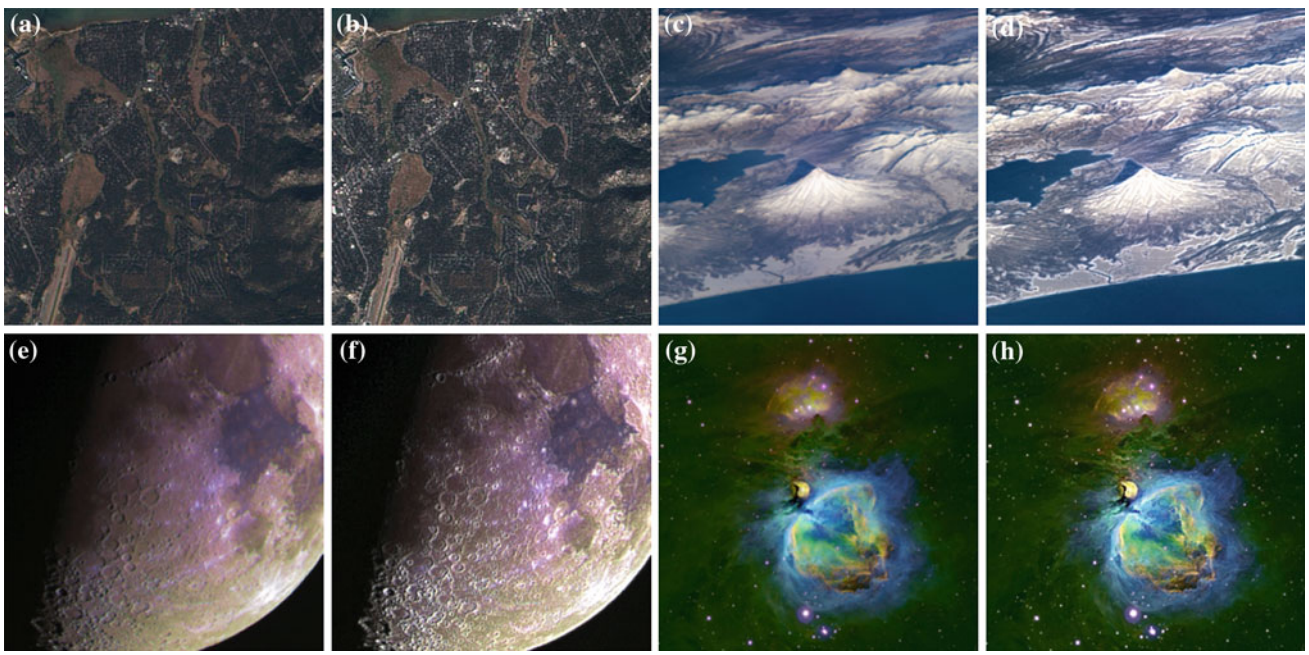

Fig. 3 Comparison between the original image and the enhanced image. **a** Lake Tahoe. **b** Enhanced image with $\alpha = 0.29$. **c** Kamchatka Volcanoes. **d** Enhanced image with $\alpha = 0.47$. **e** Moon. **f** Enhanced image with $\alpha = 0.53$. **g** Orion Nebulae. **h** Enhanced image with $\alpha = 0.3$

its processed image calculated by the 2-D DFOSGD-based image-enhancing method with the optimized $\alpha = 0.53$. It is easy to observe that the processed image has the better observability rather than the original image. The surface topography is enhanced and the stereoscopic parallax becomes more obvious. Figure 3g is an astro-photograph of the Orion Nebula downloaded from [30], and its processed image calculated by the 2-D DFOSGD-based image-enhancing method with the optimized $\alpha = 0.3$ is shown in Fig. 3h. The color of the Orion Nebula becomes more abundant, and the interstellar medium can be observed more clearly.

From these results, we can conclude that the proposed 2-D DFOSGD-based image-enhancing method can be used to enhance the given image signal.

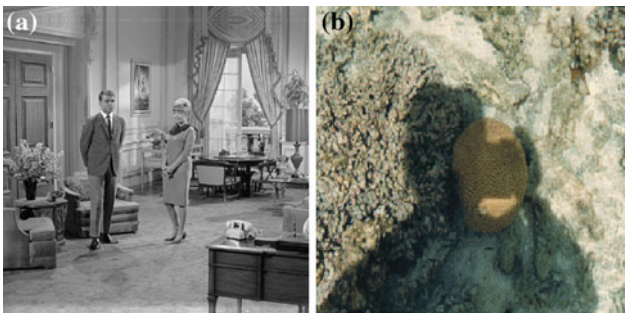

Fig. 4 Original image. **a** "Couple" image. **b** "Shadow" image

4.2 Experiment 2

In this experiment, two images are given to assess the validity of the proposed unsupervised optimization algorithm for calculating the fractional-order parameter α. Figure 4 shows the two original images. Figure 4a is the famous gray image "Couple", and Fig. 4b is the typical color image "Shadow". The proposed 2-D DFOSGD-based image-enhancing algorithms with the different α's are used to enhance these two images. The comparison results are shown in Fig. 5. Figure 5a is the enhanced image when $\alpha = 0.1$. It is almost the same with the original image and the enhancement effect is not obvious. Figure 5b is the enhanced image when $\alpha = 0.5$, and its enhancement effect is better than that of Fig. 5a. However, the contrast is not satisfactory due to the increase in the brightness of the whole image. From Fig. 5c, it is easy to see that the image is over-enhanced when $\alpha = 0.9$, and most of the detail information is covered by the saturated pixels. These results are consistent with the results of Fig. 2. Figure 5d is the enhanced image calculated by using the optimized α which is 0.32. It is obvious that its enhancement effect and contrast are better than those of the other three enhanced images. Similarly, Fig. 5e–g show the enhanced images with $\alpha = 0.1$, $\alpha = 0.5$, and $\alpha = 0.9$, respectively. The enhancement effect increases firstly and then decreases. Figure 5h is the enhanced image calculated by using the optimized α which is 0.28. It can be seen that its enhancement effect and contrast are better than those of the other three enhanced images.

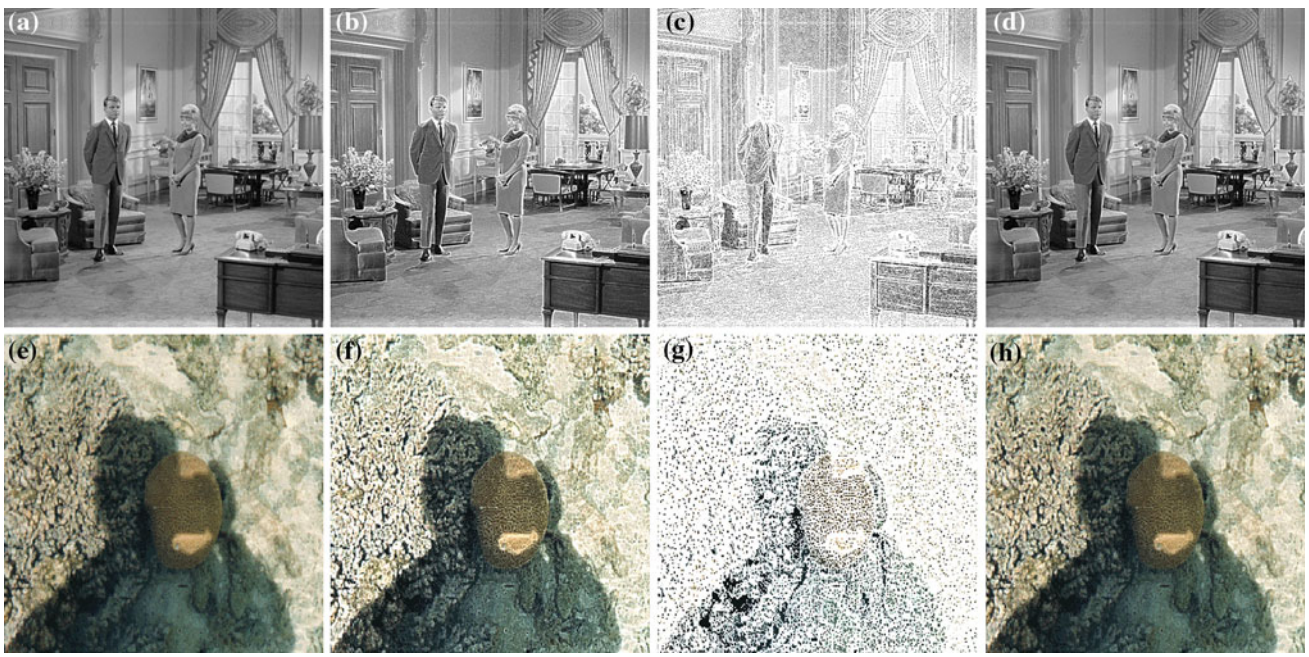

Fig. 5 Comparison between four enhanced images with different α's. **a** Enhanced image with $\alpha = 0.1$. **b** Enhanced image with $\alpha = 0.5$. **c** Enhanced image with $\alpha = 0.9$. **d** Enhanced image with $\alpha = 0.32$. **e** Enhanced image with $\alpha = 0.1$. **f** Enhanced image with $\alpha = 0.5$. **g** Enhanced image with $\alpha = 0.9$. **h** Enhanced image with $\alpha = 0.28$

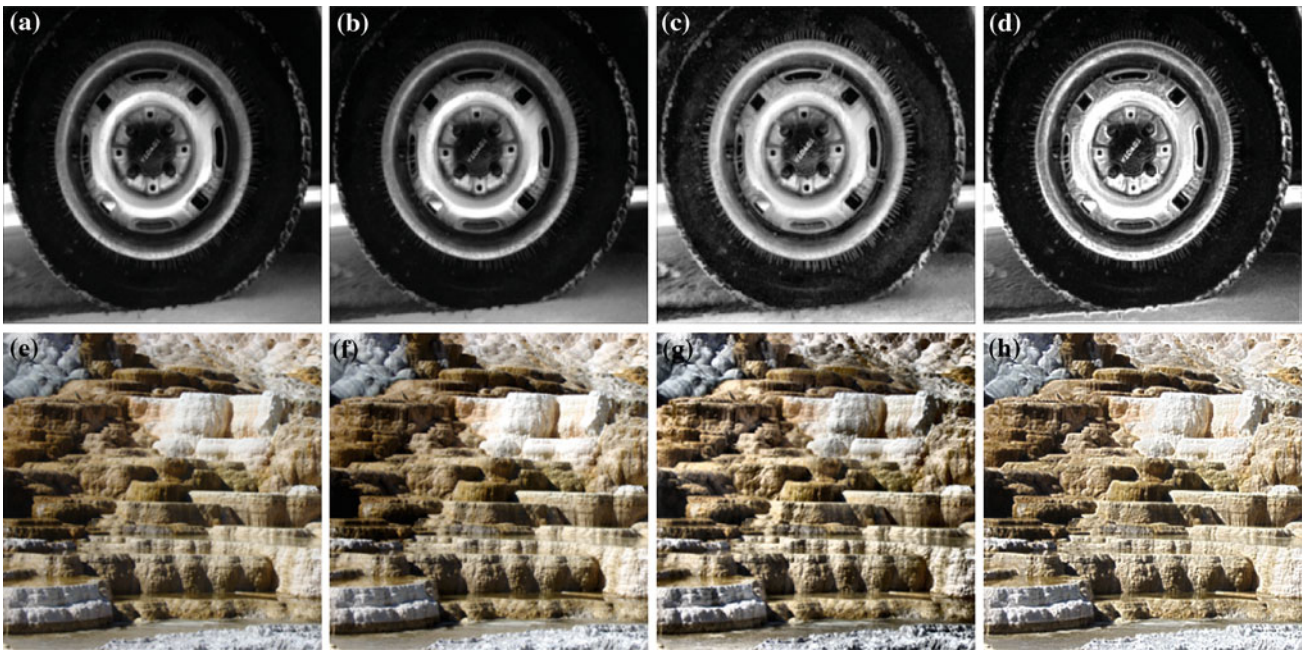

Fig. 6 Comparison between the proposed image enhancement method and two typical image enhancement methods. **a** "Tire". **b** Imadjust method. **c** Adapthisteq method. **d** The proposed method. **e** "Minerva Terrace". **f** Imadjust method. **g** Adapthisteq method. **h** The proposed method

These experimental results demonstrate the validity of the proposed unsupervised optimization algorithm.

4.3 Experiment 3

The purpose of this experiment is to compare the proposed 2-D DFOSGD-based image-enhancing method with two typical enhancing methods to evaluate their performances. The final results are shown in Fig. 6. The fractional-order α is optimized by Eq. (18), and the optimized fractional-order α is 0.49 for gray image experiment and the optimized fractional-order α is 0.37 for color image experiment. Figure 6a is the "tire" image that is usually used to evaluate the performance of the different enhancing methods. Figure 6b shows the "imadjust" [31] method's enhanced image that does not have the obvious change comparing with the original image. Figure 6c shows the "adapthisteq" [31] method's enhanced image that causes a drastic but exaggerated change. It is obvious that many detail components are covered. From Fig. 6d, it is easy to observe that the 2-D DFSG method provides a better enhanced result rather than the other two methods. For example, the texture of tire surface is more obvious and the steel ring is more rich and lustrous. Moreover, one color image experiment result is also given. Figure 6e is the photograph of the famous "Minerva Terrace" captured in Yellow Stone National Park. Similarly, Fig. 6f–h show the enhanced images by three different enhancing algorithm. Figure 6f is almost the same with the original image. Figure 6g shows a better enhanced result than Fig. 6f; especially, it shows more distinct details on the up-right and down-right corners. However, it changes the distribution of the image histogram. In other words, "adapthisteq" algorithm changes the brightness distribution in image. From Fig. 6e, we can see that the brightness of right part is bigger than that of left part in the original image because the reflective ability of white object is better than that of dark object. From Fig. 6g, we cannot get these types of information because the nature of the image is distorted. From Fig. 6h, we can see that not only is the image contrast enhanced, but also the brightness distribution in image is protected. The texture is clear and the gradation is distinct.

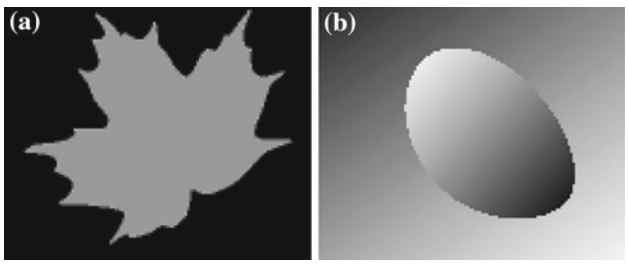

Fig. 7 Original image. **a** "Leaf" image. **b** "Degrade" image

Hence, we can conclude that 2-D DFOSGD has the better performance than "imadjust" and "adapthisteq" methods.

4.4 Experiment 4

Image enhancement technology not only can improve the observability of the image, but also can increase the accuracy

Table 1 PSNR comparison between the original image and enhanced images

	Figure 7a			Figure 7b		
Image	Chan and Vese	Li	Shi	Chan and Vese	Li	Shi
Original	21.36 (3)	23.12 (2)	19.92 (4)	9.07 (3)	12.73 (2)	8.43 (4)
Enhanced by "Imadjust" method	21.11 (4)	21.73 (4)	20.94 (3)	8.99 (4)	12.63 (3)	8.47 (2)
Enhanced by "Adapthisteq" method	21.46 (2)	21.89 (3)	21.61 (2)	10.89 (1)	7.43 (4)	9.55 (1)
Enhanced by proposed method	23.93 (1)	23.97 (1)	23.97 (1)	9.30 (2)	12.92 (1)	8.46 (3)

of some postprocessing technologies. In this experiment, three published image segmentation algorithms, Chan and Vese [32], Li [33], and Shi [34], are used to segment the original image and the enhanced images respectively, and then the segment results are evaluated using PSNR criteria, which is defined by

$$\mathrm{PSNR} = 10\log_{10}\frac{d}{\mathrm{MSE}(A,\,B)}, \tag{19}$$

where A and B are the reference mask region and the result mask region of an algorithm, d is the maximum of the image and $\mathrm{MSE}(A,\,B)$ is the mean square error defined by

$$\mathrm{MSE}(A,\,B) = \frac{1}{\mathrm{MN}}\sum_{m=1}^{M}\sum_{n=1}^{N}\|A(m,n) - B(m,n)\|^2. \tag{20}$$

Two gray images, "Leaf" and "Degrade" shown in Fig. 7, are chosen as the original image, and the corresponding enhanced images are calculated by "Imadjust" algorithm, "Adapthisteq" algorithm, and our proposed algorithm with $\alpha = 0.3$.

Table 1 shows the PSNR comparison between the original image and enhanced images. The bigger PSNR is, the better the segmentation is. The number in bracket shows the rank of the segmentation result. From the table, we can get the following conclusions. Firstly, the PSNR values of the enhanced image calculated by our proposed algorithm are all bigger than those of the corresponding original image for the three different image segment algorithms. It demonstrates that our proposed 2-D DFOSGD-based image-enhancing algorithm is helpful for improving the accuracy of some image segment algorithms. Secondly, although the "Imadjust" and "Adapthisteq" algorithms are helpful for some segment algorithms, they are not helpful for all the segment algorithms. For example, "Adapthisteq" algorithm is helpful for the Chan and Vese algorithm and Shi algorithm, but not helpful for Li algorithm. Finally, it is obvious that the best PSNR values are obtained by our proposed enhancing algorithm for the two images.

5 Conclusion

This paper firstly introduced the one-dimension digital fractional-order Savitzky–Golay differentiator (1-D DFOSGD) that generalized the traditional Savitzky–Golay filter from the integer order to the fractional order. Secondly, the 1-D DFOSGD was extended to 2-D by defining a group of direction operators, and a 2-D DFOSGD-based image-enhancing algorithm was proposed. Then, an unsupervised optimization algorithm was proposed for choosing the fractional-order parameter. Numerical experiments were performed to evaluate the performance of 2-D DFOSGD-based image-enhancing algorithm, and the results demonstrated its validity. The paper includes the following contributions. Firstly, the 1-D DFOSGD is extended to 2-D. Secondly, a new image-enhancing method based on 2-D DFOSGD is proposed, and it has very satisfying image-enhancing effect. In addition, an unsupervised optimization algorithm is proposed for choosing the fractional-order parameter. Future work involves the hardware implementation.

Acknowledgements The work of D. Chen was supported by the National Natural Science Foundation of China (No. 61174145) and the Fundamental Research Funds for the Central Universities (N110304001 and N110804005).

References

1. Oldham, K.B., Spanier, J.: The Fractional Calculus. Academic, New York, NY (1974)
2. Riemann, B.: Versuch einer allgemeinen auffassung der integration und differentiation. Gesammelte Mathematische Werke, pp. 331–344 (1876)
3. Miller, K.S.: Derivatives of noninteger order. Math. Mag. **68**(3), 183–192 (1995)
4. Caputo, M.: Linear models of dissipation whose Q is almost frequency independent-II. Geophys. J. R. Astron. Soc. **13**(5), 529–539 (1967)
5. Vinagre, B.M., Podlubny, I., Hernandez, A., Feliu, V.: Some approximations of fractional order operators used in control theory and applications. J. Frac. Calc. Appl. Anal. **4**, 47–66 (2001)
6. Podlubny, I., Petras, I., Vinagre, B.M., O'Leary, P., Dorcak, L.: Analogue realizations of fractional-order controllers. Nonlinear Dyn. **29**(1–4), 281–296 (2002)
7. Carlson, G., Halijak, C.: Approximation of fractional capacitors $(1/s)^{1/n}$ by a regular Newton process. In: IEEE Trans. Circuit Theory **11**(2), 210–213 (1964)
8. Dutta Roy, S.C.: On the realization of a constant-argument immittance or fractional operator. In: IEEE Trans. Circuit Theory **14**(3), 264–274 (1967)
9. Chareff, A., Sun, H.H., Tsao, Y.Y., Onaral, B.: Fractal system as represented by singularity function. In: IEEE Trans. Autom. Control **37**(9), 1465–1470 (1992)

10. Matsuda, K., Fujii, H.: H_∞ optimized wave-absorbing control: analytical and experimental results. J. Guid. Control Dyn. **16**(6), 1146–1153 (1993)
11. Oustaloup, A., Levron, F., Mathieu, B., Nanot, F.M.: Frequency-band complex noninteger differentiator: characterization and synthesis. In: IEEE Trans. Circuits Syst. I Fundam. Theory Appl. **47**(1), 25–39 (2000)
12. Tseng, C.-C.: Design of fractional order digital FIR differentiators. IEEE Signal Process. Lett. **8**(3), 77–79 (2001)
13. Samadi, S., Ahmad, M.O., Swamy, M.N.S.: Exact fractional-order differentiators for polynomial signals. IEEE Signal Process. Lett. **11**(6), 529–532 (2004)
14. Chen, Y.Q., Moore, K.L.: Discretization schemes for fractional-order differentiators and integrators. IEEE Trans. Circuits Syst. I Fundam. Theory Appl. **49**(3), 363–367 (2002)
15. Chen, Y.Q., Vinagre, B.M.: A new IIR-type digital fractional order differentiator. Signal Process. **83**(11), 2359–2365 (2003)
16. Tseng, C.-C.: Improved design of digital fractional-order differentiators using fractional sample delay. IEEE Trans. Circuits Syst. I Regul. Pap. **53**(1), 193–203 (2006)
17. Barbosa, R.S., Tenreiro Machado, J.A., Silva, M.F.: Time domain design of fractional differintegrators using least-squares. Signal Process. **86**(10), 2567–2581 (2006)
18. Tenreiro Machado, J.A., Galhano, A.M., Oliveira, A.M., Tar, J.K.: Approximating fractional derivatives through the generalized mean. Commun. Nonlinear Sci. Numer. Simul. **14**(11), 3723–3730 (2009)
19. Tseng, C.C., Lee, S.L.: Design of fractional order digital differentiator using radial basis function. IEEE Trans. Circuits Syst. I Regul. Pap. **57**(7), 1708–1718 (2010)
20. Tenreiro Machado, J.A.: Calculation of fractional derivatives of noisy data with genetic algorithms. Nonlinear Dyn. **57**(1–2), 253–260 (2009)
21. Chen, D.L., Chen, Y.Q., Xue, D.Y.: Digital fractional order Savitzky-Golay differentiator. IEEE Trans. Circuits Syst. II Express Briefs **58**(11), 758–762 (2011)
22. Bai, J., Feng, X.C.: Fractional-order anisotropic diffusion for image denoising. IEEE Trans. Image Process. **16**(10), 2492–2502 (2007)
23. Oustaloup A., Mathieu B., Melchior P. (1991) Edge detection using non integer derivation. In: IEEE European Conference on Circuit Theory and Design, pp. 3–6
24. Mathieu, B., Melchior, P., Oustaloup, A., Ceyral, C.: Fractional differentiation for edge detection. Signal Process. **83**, 2421–2432 (2003)
25. Pu, Y.F., Wang, W., Zhou, J.L.: Fractional differential approach to detecting textural features of digital image and its fractional differential filter implementation. Sci. China Ser. E Inf. Sci. **38**(2), 2252–2272 (2008)
26. Chen, D.L., Chen, Y.Q., Xue, D.Y.: Digital fractional order Savitzky-Golay differentiator and its application. In: Proceedings of the ASME 2011 International Design Engineering Technical Conferences and Computers and Information in Engineering Conference, pp. 1–10 (2011)
27. Pu, Y.F., Zhou, J.L., Yuan, X.: Fractional differential mask: a fractional differential based approach for multi-scale texture enhancement. IEEE Trans. Image Process. **19**(2), 491–511 (2010)
28. Gonzalez, R.C., Woods, R.E.: Digital Image Processing. 2nd edn. Prentice Hall, New Jersey (2002)
29. http://earthobservatory.nasa.gov/
30. http://bf-astro.com/
31. Gonzalez, R.C., Woods, R.E., Eddins, S.L.: Digital Image Processing Using MATLAB. 2nd edn. Gatesmark, Knoxville, TN (2009)
32. Chan, T.F., Vese, L.A.: Active contours without edges. In: IEEE Trans. Image Process. **10**(2), 266–277 (2001)
33. Li, C., Kao, C.Y., Gore, J.C., Ding, Z.: Minimization of region-scalable fitting energy for image segmentation. In: IEEE Trans. Image Process. **17**(10), 1940–1949 (2008)
34. Shi, Y., Karl, W.C.: A real-time algorithm for the approximation of level-set-based curve evolution. In: IEEE Trans. Image Process. **17**(5), 645–656 (2008)